ACS APPLIED MATERIALS & INTERFACES

www.acsami.org

Research Article

Highly Flexible Multilayered e-Skins for Thermal-Magnetic-Mechanical Triple Sensors and Intelligent Grippers

Shuai Liu, Sheng Wang,* Shouhu Xuan, Shuaishuai Zhang, Xiwen Fan, Han Jiang, Pingan Song,* and Xinglong Gong*

Cite This: *ACS Appl. Mater. Interfaces* 2020, 12, 15675−15685

Read Online

ACCESS | Metrics & More | Article Recommendations | Supporting Information

ABSTRACT: This work reports a novel triple-functional electronic skin (e-skin) which shows both wonderful thermal−magnetic−mechanical sensing performance and interesting magnetic actuation behavior. The flexible e-skin comprises thermo-sensitive, magnetic, and conductive tri-components, and their sensitive characteristics under 5−70 °C, 0−1200 mT, and 0.1−5.1 MΩ are studied, respectively. Owing to the unique piezoresistive characteristic and magnetorheological effect, the e-skin exhibits a rapid response time (38 ms) to the external stimuli. The assembled e-skin with the triple-layer structure can act as a functional sensor to monitor various human motions, magnetic fields, and environmental temperatures. Based on this e-skin, an intelligent magneto-active gripper is further developed, and it can be used to grasp and transport targets by the actuated force of magnetic field under various working conditions. Importantly, the multi-functional sensing capability endows the gripper with real-time deformation and ambient temperature perception characteristics. As a result, because of the ideal multi-field coupling sensing and magnetic active features, this e-skin shows a wide prospect in wearable electronics, man−machine interactions, and intelligent transport systems.

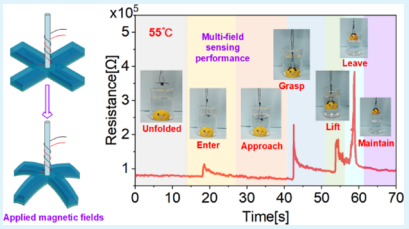

KEYWORDS: *e-skin, thermal−magnetic−mechanical monitoring, magnetic actuation, intelligent gripper*

1. INTRODUCTION

Human skin, which plays a vital role in the interaction between individuals and surroundings, can monitor various external stimuli, such as temperature,[1] humidity,[2] tactile touch,[3] and pressure.[4] With the rapid development of artificial intelligence,[5] medical health,[6] and sports monitoring,[7] electronic skins (e-skins), with superior sensitivity and reliable performance, have been developed to mimic and further functionalize nature skins. Commonly, e-skins include piezoresistivitive,[8,9] piezoelectricitive,[10,11] capacitive,[12,13] and triboelectric[14,15] types, in which piezoresistive e-skin has gained more attention due to facile preparation and high sensitivity. They are usually derived from flexible polymer substrates[9] and conductive carbon/metal fillers.[16−19] Especially, Ecoflex rubber with high flexibility and stretchability has been successfully applied as a biocompatible matrix in various e-skins.[20−22] A multilayer graphene epidermal e-skin was fabricated by packing laser scribing graphene into Ecoflex, and it exhibited excellent strain-sensitive performance.[20] By transferring Ag ink onto stretchable Ecoflex/hydrogel substrates, a polymer conductor with ultrastretchable property and ideal sensing ability showed promising applications as e-skin electronics.[21]

Intelligent materials, which are capable of adapting themselves to the environment under applied force,[23] light,[24] magnetism,[25] and heat[26] stimuli, have gained extensive attention because of their wide application. Recently, owing to the unique stimuli-responsive performance, they have been extensively introduced into flexible Ecoflex-based e-skins which endow them with novel functions. For instance, an all-polymer-based polymorph skin with a soft Ecoflex actuator was reported, and it possessed fully electrically controllable surface for friction or flow control.[27] A variable transmittance skin, developed by integrating carbon nanotubes and stretchable Ecoflex film, showed intelligently responsive ability to the applied strain by adjusting its transmittance.[28] To meet the requirement of the artificial muscle, both sensitive and actuating functions should be integrated together within the next-generation of multi-functional e-skin electronics.

Magneto-actuation is attractive in the soft intelligent robots because of its non-contact, fast, continuous, and reversible conduction. As a typical magneto-active material, magneto-rheological elastomers (MREs)[29] are attractive in actuation because their mechanical properties such as storage modulus and stiffness can be controlled by magnetic field.[30] During the past decades, several kinds of MRE-based actuators have been developed, and they showed wonderful magneto-actuation performance.[31,32] Recently, a novel conductive MRE-based sensor was reported, and besides sensing mechanical strains, it could also respond to the excitation of magnetic field.[33]

Received: December 31, 2019
Accepted: March 5, 2020
Published: March 5, 2020

Downloaded via UNIV SCIENCE AND TECHNOLOGY CHINA on April 9, 2020 at 05:44:02 (UTC).
See https://pubs.acs.org/sharingguidelines for options on how to legitimately share published articles.

© 2020 American Chemical Society

https://dx.doi.org/10.1021/acsami.9b23547
ACS Appl. Mater. Interfaces 2020, 12, 15675−15685

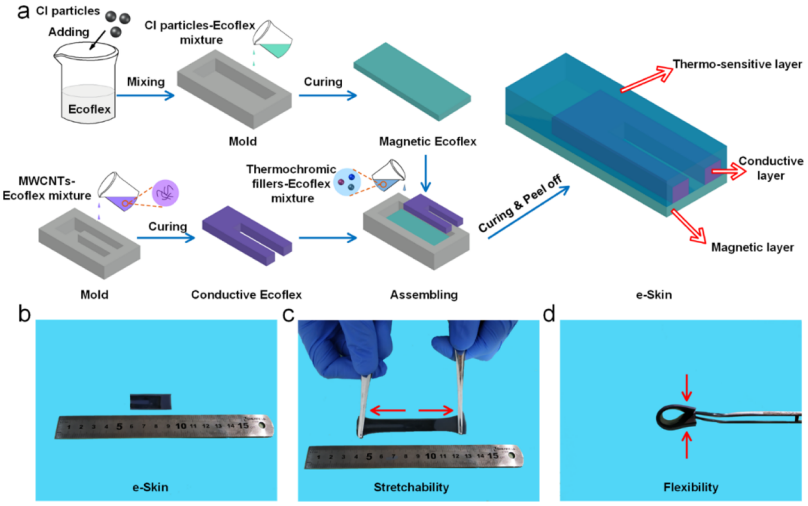

Figure 1. (a) Fabrication procedures of the e-skin. (b) As-prepared e-skin with (c) stretchability and (d) flexibility.

Moreover, a cantilever micro-electro-mechanical system actuator was created by using sandwich structures with an MRE core, which successfully accomplished the pull-in voltage control under the excitation of magnetic field.[34] Obviously, besides the sensing behavior, the e-skins prepared by the MREs also exhibit magneto-actuated characteristics. As a result, the development of novel e-skins with controllable stimuli-responsive property can be achieved by using multi-functional MREs.

Although various versatile e-skins have gained considerable development, it remains as a crucial issue to expand the detection categories, which has limited their wider applications.[35] With the rapid growth of soft robotics, an urgent demand is proposed for smart sensors with multi-functional sensitivity to temperature, pressure, and deformation.[36] Besides, the perception and actuation performance toward magnetic field, which contributes to contactless drive and precise control, need to be improved.[37] According to our knowledge, the e-skins reported previously may not meet such requirements. Especially, the e-skin integrated with thermal−magnetic−mechanical monitoring capability and magneto-actuated effect, which is expected to be an effective strategy to promote the development of relevant research, has not been reported yet.

In this work, a novel e-skin with multiple functional layers, which could sense thermal−magnetic−mechanical stimuli, was facilely fabricated by the integration of Ecoflex composites with the thermo-sensitive, magnetic, and conductive characteristics. The flexible e-skin functioned as a wearable device by detecting various motions such as slight touch, bending, compressions, and magnetic fields. It also possessed good thermal sensitivity which could sense external temperature variations. Furthermore, an e-skin-based intelligent gripper was also developed, which could capture and transport objects owing to the magneto-actuated characteristic. Based on the sensitive resistance variations, it also showed stable detection ability to the deformations and working temperatures in the process. Finally, the e-skin possessed high potential in the development of multi-functional wearable electronics.

2. EXPERIMENTAL SECTION

2.1. Materials. The multi-walled carbon nanotubes (MWCNTs) with a diameter of 8−13 nm and length of 3−12 μm were provided by conductive materials of Heluelida Power Sources Co., Ltd., Xinxiang City, Henan Province, China. The carbonyl iron particles (CI particles, CN-type) with the diameter of about 7 μm were purchased from BASF Aktiengesellschaft, Germany. The commercially available thermochromic fillers were bought from Shenzheng Bianse Chemical Technology Co., Ltd., China. The silicone rubber Ecoflex 00-30 was purchased from Smooth-On, PA, USA.

2.2. Preparation of Thermosensitive Ecoflex, Magnetic Ecoflex, and Conductive Ecoflex Composites. First, Ecoflex 00-30 A and B were placed into a beaker (a mass ratio of 1:1) as the polymer matrix. Then, the thermochromic fillers (the mass ratio of thermochromic red, blue, and black fillers was 3:1:1) were added, followed by homogeneously stirring the mixture for 5 min. The prepared thermochromic filler−Ecoflex mixture was poured into the mold and degassed in a vacuum chamber for 10 min. The preparation method of CI particle−Ecoflex and MWCNT−Ecoflex mixture was the same as the abovementioned mixture. Afterward, thermo-sensitive Ecoflex and conductive Ecoflex were prepared by curing the corresponding mixture in an oven for 4 h at 60 °C, while magnetic Ecoflex was obtained after being cured at room temperature for 4 h.

2.3. Fabrication of the e-Skin and Intelligent Gripper. The cured magnetic Ecoflex (40 mm × 15 mm × 0.2 mm) was first put at the bottom of the mold (40 mm × 15 mm × 1 mm). The cured U-shaped conductive Ecoflex (each arm was linked up with a copper wire) was then placed. Afterward, the thermochromic filler−Ecoflex mixture was poured into the mold, followed by degassing for 10 min. After being cured for 4 h at 60 °C, this novel e-skin was acquired.

In addition, an e-skin-based intelligent gripper with four arms was further manufactured. The magnetic Ecoflex and conductive Ecoflex were molded into cross shape (the size of each arm is 20 mm × 10 mm × 0.2 mm) and U shape, respectively. The assembly method was the same as that mentioned above.

2.4. Characterization. The micro-morphologies of materials were characterized by a scanning electron microscope (Gemini 500, Carl Zeiss Jena, Germany). The rheological properties of the magnetic Ecoflex were studied by a rheometer (Physica MCR 301, Anton Paar Co., Austria) with an external magnetic field system. In this study, a paralleled plate rotor with a diameter of 20 mm was adopted, and the gap was set at 1 mm. The tested samples were molded into cylinders with a thickness of about 1 mm and diameter of 20 mm, respectively. During the magnetorheological performance measurement, an external coil was used to generate controllable magnetic field, and the magnetic flux density ranged from 0 to 1200 mT by varying the current of 0−5 A. The testing temperature was maintained at 25 °C, and the oscillation strain and frequency was set at 0.1% and 1 Hz, respectively. A magnetic property measuring system vibrating sample magnetometer (SQUID, Quantum Design Co., America) was used to test the magnetic hysteresis loops. The electrical properties were

https://dx.doi.org/10.1021/acsami.9b23547
ACS Appl. Mater. Interfaces 2020, 12, 15675−15685

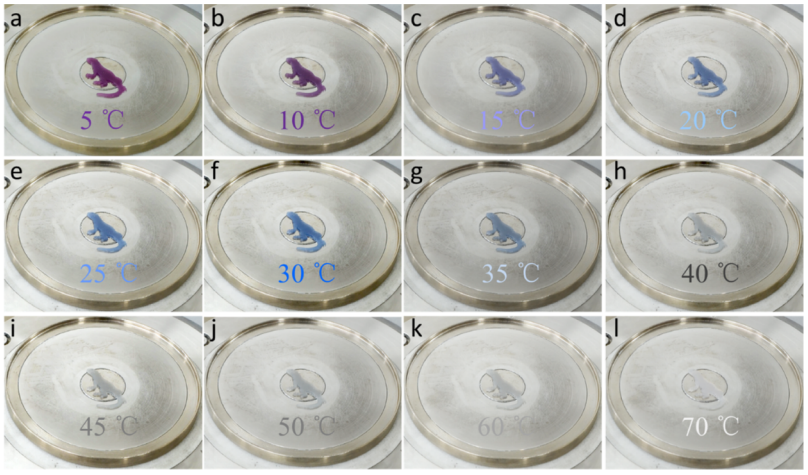

Figure 2. Temperature-sensing effect of thermo-sensitive Ecoflex by visual color changes in the range of 5−70 °C.

measured by a ModuLab material test system (MTS) (Solartron analytical, AMETEK advanced measurement technology, Inc., United Kingdom). The applied force and displacement were controlled by an MTS (criterion 43, MTS System Co., America).

3. RESULTS AND DISCUSSION

3.1. Materials Design and Structural Characterizations. The fabrication processes of this e-skin are schematically illustrated in Figure 1a. In brief, CI particles and MWCNTs were uniformly dispersed in Ecoflex and then degassed and cured. Next, the cured materials were assembled onto the prepared mold, followed by pouring the thermochromic filler−Ecoflex mixture. Finally, they were vulcanized, and a stable triple-layer structured e-skin was obtained (Figure 1b). Originated from Ecoflex rubber, the e-skin showed stretchable characteristic (Figure 1c). Besides, it could be bent easily, exhibiting favorable flexibility (Figure 1d).

The micro-morphologies of the materials are shown in Figure S1. Figure S1a−c reveals that red, blue, and black fillers exhibited similar structures with a size distribution of 3−7 μm. As shown in Figure S1d, CI particles presented spherical morphologies with an average diameter of about 7 μm. Large numbers of MWCNTs and the bundles are observed in Figure S1e, and they were beneficial for forming effective conductive paths (ECPs) in the final conductive Ecoflex.[38] Figure S1f−i presented the scanning electron microscopy (SEM) images of pure Ecoflex rubber, thermo-sensitive Ecoflex, magnetic Ecoflex, and conductive Ecoflex, respectively. It was evident that the surface of pure Ecoflex was smooth, while the incorporation of functional fillers increased the surface roughness of all composites. The homogenous distribution of nanofillers could be observed in the section view which guaranteed reliable mechanical properties.

3.2. Thermosensation Properties of Thermo-Sensitive Ecoflex. Owing to the dramatic response to temperatures, the thermochromic fillers in ethanol solutions could change their colors from bright to colorless as the external temperature rose (Figure S2), showing ideal temperature-sensitive performance. Obviously, the temperature sensing ranges of red, blue, and black fillers were 5−25, 15−40, and 40−65 °C, respectively. The temperature-dependent color of chameleon-shaped thermo-sensitive Ecoflex is shown in Figure 2. The color changed from violet (5 °C), indigo (20−30 °C), light grey (40−60 °C) to colorless (70 °C), indicating its wide temperature-responsive region. Besides, when the temperature dropped, the color exhibited favorable reversibility (Figure S3). Therefore, thermo-sensitive Ecoflex was expected to be applied to the evaluation of ambient temperatures.

3.3. Magnetic-Mechanical Coupling Properties of Magnetic Ecoflex. Magnetic Ecoflex presented remarkable responsive characteristics to magnetic field due to the presence of CI particles. For convenience, magnetic Ecoflex composites with different CI contents were defined as magnetic Ecoflex-X, where X was the mass fraction of CI particles. Figure 3a shows the hysteresis loops of magnetic Ecoflex, pure Ecoflex, and CI particles. CI particles displayed typical soft magnetic property

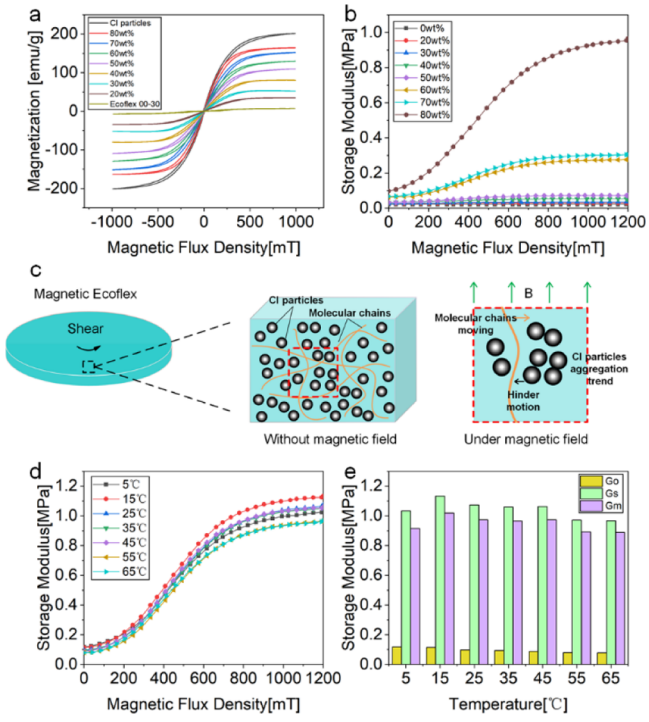

Figure 3. (a) Magnetic hysteresis loops of magnetic Ecoflex, pure Ecoflex, and CI particles. (b) Storage modulus of magnetic Ecoflex with different CI mass fractions as a function of magnetic flux density. (c) Magnetorheological property measurement and the schematic diagram. (d) Temperature-dependent MR effects of magnetic Ecoflex-80%. (e) G_o, G_s, and G_m vs temperature.

https://dx.doi.org/10.1021/acsami.9b23547
ACS Appl. Mater. Interfaces 2020, 12, 15675−15685

with a saturated magnetization intensity of 201.3 emu/g, while Ecoflex rubber was non-magnetic. As CI contents increased from 20 to 80 wt %, the saturated magnetization intensity of magnetic Ecoflex gradually raised from 34.7 to 163.9 emu/g, indicating a significantly increased magnetic responsive property.

As reported previously,[39,40] magnetic field stimulation could influence the rheological properties of MREs; so the magnetic-induced mechanical performance of magnetic Ecoflex was studied by a rotational rheometer. Figure 3b depicts the storage modulus of magnetic Ecoflex as a function of applied magnetic fields. To compare the magnetic-induced behaviors, we defined the magnetorheological (MR) effect as

$$\text{MR effect} = \frac{G_m}{G_o} \times 100\% = \frac{G_s - G_o}{G_o} \times 100\% \quad (1)$$

in which G_o and G_s are the initial and largest storage modulus during the test, and thus G_m is the magnetic-induced modulus. The details are listed in Table 1. Obviously, the storage modulus of all magnetic Ecoflex composite rose with the increase of magnetic flux density and finally tended to be saturated. As shown in Figure 3c, this phenomenon was attributed to the formation of CI particle aggregates, and the interaction force between particle aggregates under the magnetic field which further impeded the movement of polymer chains.[29] Meanwhile, CI content showed a positive effect on the MR effect. As the content ranged from 20 to 80 wt %, the corresponding MR effect increased from 11.1 to 893.8% and G_s values were 2.9×10^{-3} and 8.7×10^{-1} MPa (under 1200 mT magnetic flux density) respectively, indicating a significant enhancement in mechanical properties. In summary, the mechanical performance could be regulated rapidly and reversibly by magnetic field, which was meaningful for magnetic actuation and control engineering.

Table 1. G_o, G_s, G_m, and MR Effect of Magnetic Ecoflex Composites with Different CI Mass Fractions

CI mass fraction [%]	G_o [MPa]	G_s [MPa]	G_m [MPa]	MR effect [%]
0	2.06×10^{-2}	2.11×10^{-2}	4.70×10^{-4}	2.28
20	2.60×10^{-2}	2.89×10^{-2}	2.89×10^{-3}	11.12
30	2.62×10^{-2}	3.49×10^{-2}	8.74×10^{-3}	33.40
40	3.21×10^{-2}	5.22×10^{-2}	2.00×10^{-2}	62.29
50	3.24×10^{-2}	7.19×10^{-2}	3.95×10^{-2}	121.86
60	6.16×10^{-2}	2.77×10^{-1}	2.16×10^{-1}	350.20
70	6.66×10^{-2}	3.05×10^{-1}	2.38×10^{-1}	358.16
80	9.72×10^{-2}	9.66×10^{-1}	8.69×10^{-1}	893.83

Moreover, the temperature-dependent MR performance of magnetic Ecoflex-80% was studied owing to its importance for applications (Figure 3d,e). When the temperature increased from 5 to 65 °C, G_o showed a slight decrement, while G_s and G_m fluctuated modestly. Overall, magnetic Ecoflex-80% presented a high MR effect, which endowed it with the potential of magnetocontrollable performance, and the thermal−mechanical stability was also beneficial for its practical applications.

3.4. Mechanical−Electrical Coupling Sensing Properties of Conductive Ecoflex. Owing to the incorporated MWCNTs, the conductivity of the composite was necessarily studied. Figure 4a shows the impedance of conductive Ecoflex with different amounts of MWCNTs. Here, the highest MWCNT content was 4.2 wt % because more MWCNTs would destroy the curing process of the composite (Figure S4). The impedances of conductive Ecoflex with MWCNT

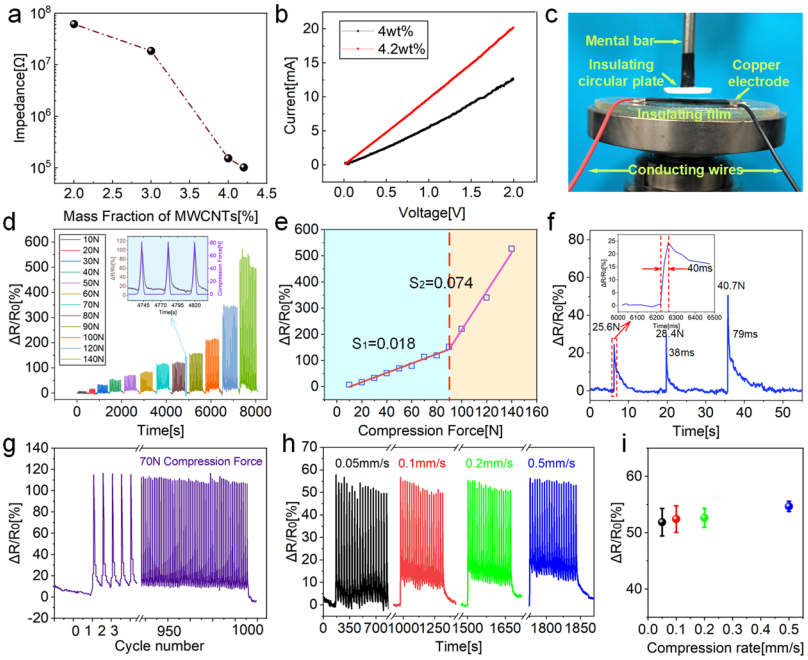

Figure 4. Electrical conductivity and compression sensing performance of conductive Ecoflex. (a) Impedance as a function of MWCNT mass fractions. (b) Current−voltage curves of conductive Ecoflex with MWCNT mass fractions of 4 and 4.2%. (c) Photographs of the experimental setup in the compression test. (d) Sensing signals to different compression forces. Inset: $\Delta R/R_0$ values and compression force of 80 N as a function of time. (e) Relative resistance variation vs compression force. (f) Fast response under sudden external compression forces. Inset: A magnified view of the rise edge. (g) Cyclic stability under a repeated compression force of 70 N. (h) Sensing properties at different compression rates under 40 N. (i) Relative resistance variation vs compression rate.

https://dx.doi.org/10.1021/acsami.9b23547
ACS Appl. Mater. Interfaces 2020, 12, 15675−15685

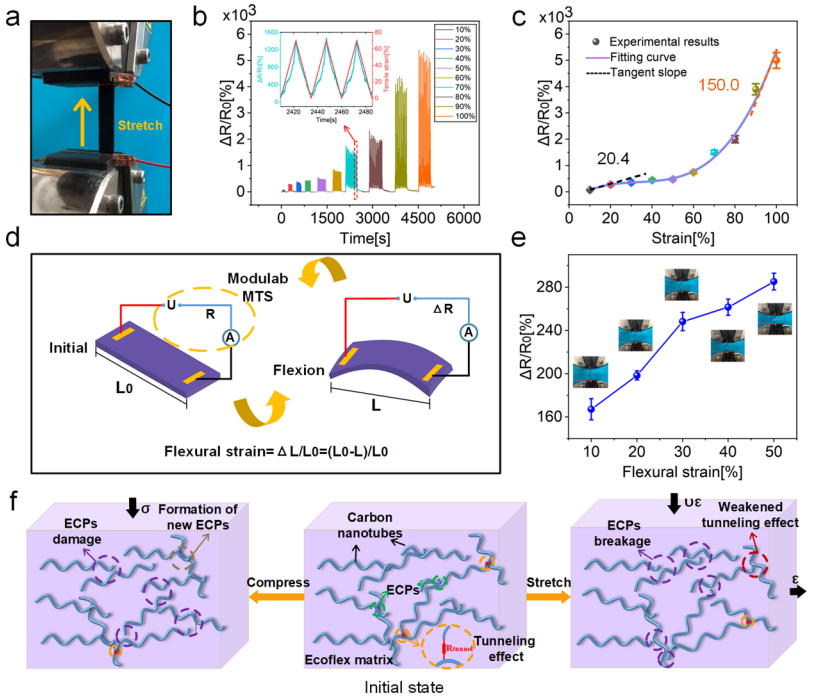

Figure 5. (a) Photographs of the tensile experimental setup. (b) Sensing signals as a function of tensile strains ranging from 0 to 100%. Inset: $\Delta R/R_0$ values and tensile strain of 70% as a function of time. (c) Relative resistance variation and GF vs tensile strain. (d) Schematic illustrations for flexion sensing measurement. (e) Relative resistance variations and photographs at different flexural strains. (f) Schematic illustrations of the conductive network evolution under compressing and stretching excitations.

contents of 3 and 4 wt % were 1.9×10^7 and 1.5×10^5 Ω, respectively, which manifested that the percolation threshold was between 3 and 4 wt %. Figure 4b indicates a linear relationship between the voltage and current of the composites, and the calculated resistances of specimens proved that MWCNTs played an essential role in enhancing the conductivity of polymer composites. Based on the above research, conductive Ecoflex-4.2% with good conductivity was a favorable candidate for a further sensing study.

Considering the effect of external force on the electrically percolated MWCNT networks, the mechanical−electrical coupling sensing performance of conductive Ecoflex-4.2% under various stimuli was systematically investigated. Compression experiments were carried out to test the dynamic response to pressure excitations (Figure 4c). The sample with a size of 50 mm × 10 mm × 1 mm was placed on an insulating polydimethylsiloxane film, and both ends were connected with copper electrodes and conductive wires. A homemade insulating circular plate with a diameter of 20 mm was applied to load the mechanical excitations. Figure 4d shows the relative resistance variation $\Delta R/R_0$ (R_0 and ΔR were the initial resistance and resistance variation respectively) as a function of time when conductive Ecoflex suffered various compression forces. Obviously, during the loading−unloading cycles, conductive Ecoflex exhibited a distinguished response with short time. The inset figure presented $\Delta R/R_0$ and compression force of 80 N as a function of time, and similar characteristics of 10, 30, and 100 N are shown in Figure S5a−c. When the compression forces were loaded, the resistance increased synchronously due to the timely deformation, and thus the hysteresis property could be almost ignored. After the forces were unloaded, the resistance decreased gradually with the release of the residual strain, presenting low hysteresis characteristics. As the compression force increased from 10 to 140 N, the corresponding relative resistance variations were 6.8, 16.3, 31.2, 50.7, 69.4, 81.9, 113.8, 118.9, 155.8, 212.4, 340.1, and 527.2%. Figure 4e shows the calculated compression force sensitivity (S), which was defined as

$$S = \frac{\delta(\Delta R/R_0)}{\delta F} \tag{2}$$

where $\delta(\Delta R/R_0)$ and δF are the increments of relative resistance variation and compression force, respectively. The plots presented two characteristic stages which corresponded to different sensitivities. In the low force region (less than 90 N), a sensitivity of 0.018 N^{-1} was displayed, indicating that $\Delta R/R_0$ possessed a favorable linear functional relationship with the compression force. In the high force region (above 90 N), the deformations were more serious, which aggravated the damage to conductive networks and made the carbon nanotubes massively disconnected. As a result, a promoted resistance increment was generated when the forces increased; so an enhanced sensitivity of 0.074 N^{-1} was presented. Besides, it showed a fast response when sudden external compression forces were applied (Figure 4f). The short response times of 40, 38, and 79 ms under compression forces of 25.6, 28.4, and 40.7 N were presented, which demonstrated that it could respond fast to external stimuli. In addition, because of the viscoelasticity of the polymer matrix, the residual strain existed after unloading external stimuli. Thus, the microstructures and resistance recovery presented a relaxation effect and the decay time of the sensor was much longer than the rise time. Fortunately, the resistance could return to the initial level, which endowed it with satisfactory reusability. To further study the cyclic stability of electrical response, a repeated compression of 70 N with 1000 cycles of load-unloading excitations was conducted on conductive Ecoflex. As shown in Figure 4g, the relative resistance variation exhibited ideal

https://dx.doi.org/10.1021/acsami.9b23547
ACS Appl. Mater. Interfaces 2020, 12, 15675−15685

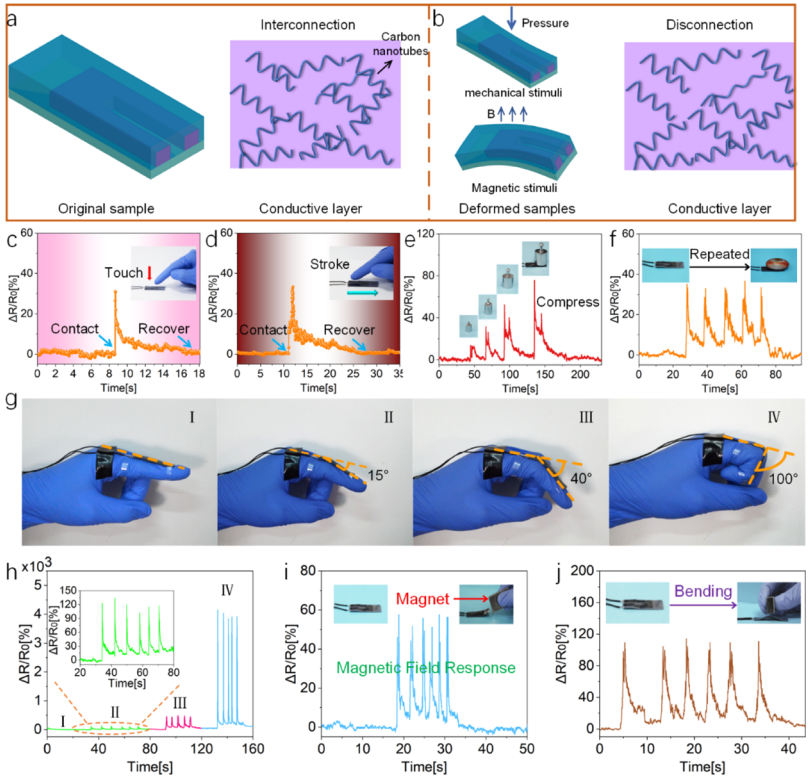

Figure 6. Multiple stimuli perception behaviors of the e-skin. (a,b) Schematic illustrations of the sample and conductive CNT networks before and after various stimuli. Sensing signals excited by (c) slight tough, (d) stroke, (e) compression by different weights, and (f) cyclic stability, (g,h) finger flexures, and magnetoactuated deformations of (i) end warping and (j) middle bending.

stability during the test, which proved conductive Ecoflex had an excellent persisting force-sensing performance.

Furthermore, it was meaningful to explore the influence of compression rates on the electrical response because the loading frequency was also important for sensors. Hence, we explored the response of conductive Ecoflex under compression of 40 N with the rates of 0.05−0.5 mm/s. The values of $\Delta R/R_0$ were 51.8 and 54.1% with the corresponding rates of 0.05 and 0.5 mm/s (Figure 4h). This increment also demonstrated that the compression rates had an enhancing effect on the sensing performance of conductive Ecoflex (Figure 4i).

To investigate the stretch-responsive properties of conductive Ecoflex, the sensing properties under different tensile loadings were evaluated. The sample was fixed on MTS, and the electrical signals were synchronously recorded (Figure 5a). Figure 5b shows the sensing performance as a function of tensile strains ranging from 0 to 100%. Under a tensile state, the resistance of conductive Ecoflex significantly increased, and it would recover after unloading the tension. As shown in the inset of Figures 5b and S5d−f, the resistance change showed good consistency with the applied tensile strains. When the tensile strain was 20%, $\Delta R/R_0$ was 282.8% (Figure S6a). With the increase of tensile strain, the corresponding $\Delta R/R_0$ could reach as high as 774.6% under 60% strain (Figure S6b) and even 5043.4% when the strain was extended to 100%. Evidently, the distinguishable outputting signals could be applied to the precise assessment of tensile strains.

To quantitatively evaluate the sensitivity to tensile strain, the gauge factor (GF)

$$\mathrm{GF} = \frac{\delta(\Delta R/R_0)}{\delta\varepsilon} \tag{3}$$

was calculated based on the measured values. As shown in Figure 5c, the GF was 20.4 within 10−20% strain and reached about 150.0 at 90−100% strain, which indicated its high monitoring sensitivity. In conclusion, conductive Ecoflex displayed excellent tensile deformation monitoring capacity with high sensitivity and reliable stability.

Owing to the high flexibility, conductive Ecoflex was also capable of monitoring flexion deformations. To explore its flexion sensitivity, various loading−unloading flexural strains were conducted (Figure 5d). It displayed considerable resistance increments and reliable stability. As the flexural strains were 10, 20, 30, 40, and 50%, the corresponding $\Delta R/R_0$ values were 167.1, 198.4, 248.2, 261.6, and 285.2%, respectively (Figure 5e). In addition, the resistance could return to initial values after unloading the excitations, indicating favorable flexion-sensing properties.

According to previous works, the force-sensing property of the polymer sensor was attributed to the destruction and reconstruction of ECPs, as well as the evolution of the tunneling effect.[41] Figure 5f displays the evolution process of the conductive network under compressing and stretching excitations. When the pressure was applied, carbon nanotubes with large aspect ratios would orient to the direction which was perpendicular to pressure.[42] In this case, the ECPs were mainly broken down, leading to a considerable increment in resistance. In the tensile process, the average distance between carbon nanotubes were dominantly increased, which caused dramatic breakage to ECPs. Moreover, the increased distance also impeded electron transitions which further weakened the

https://dx.doi.org/10.1021/acsami.9b23547
ACS Appl. Mater. Interfaces 2020, 12, 15675−15685

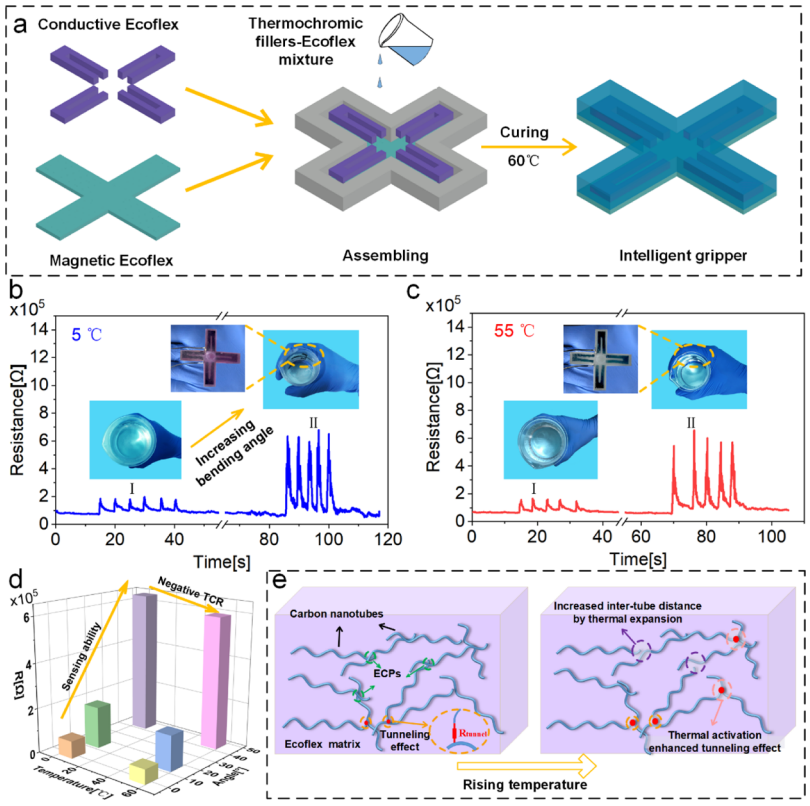

Figure 7. (a) Fabrication process of the intelligent gripper. Temperature-dependent sensing performance of the gripper at (b) 5 and (c) 55 °C. (d) Resistance comparison in different bending states. (e) Schematic diagram of the conductive networks at different temperatures.

tunneling effect. Therefore, the electrical conductivity of conductive Ecoflex was dramatically reduced when it was stretched, and ΔR showed a remarkable increment as the tensile strain further increased. In conclusion, flexible conductive Ecoflex presented excellent mechanical−electrical coupling sensing properties to compressing, stretching, and bending deformations which endowed it with great potentials in intelligent devices such as flexible sensors and versatile wearable electronics.

3.5. Multiple Stimuli Perception Behaviors of the e-Skin. Based on the effect of various external stimuli on the deformation and conductive network evolution, the assembled e-skin presented excellent sensing properties toward multiple stimuli (Figure 6a,b). The perception behaviors toward various external stimuli were explored, and the results are displayed in Figure 6. When stimulated by slight touch, it could respond instantly and recover within 8 s (Figure 6c), which illustrated its distinguished response sensitivity. However, the electrical responsive signal could hold for 15 s under stroking (Figure 6d), indicating its ideal timely monitoring capacity. Figure 6e,f shows the electrical signals stimulated by compression. The stress could be effectively assessed by the distinguished variation of $\Delta R/R_0$, and the e-skin also showed cyclic stability under repeated compression. Figure 6g,h further exhibited the human motion monitoring performance of this e-skin. The e-skin was first wore on a finger to perceive the bending deformations. With the bending angle varied from 15 to 100°, $\Delta R/R_0$ increased from 114.9 to 3940.9%. Because of the remarkable sensing characteristics, this e-skin could act as a soft wearable device in monitoring various physiological motions.

In addition, different magnetic field excitations were also applied to further explore the magneto-sensitive behavior of the e-skin. As shown in Figure 6i,j, when the magnetic field approached to the end and middle parts, the e-skin was actuated and the corresponding $\Delta R/R_0$ values were 55.9 and 109.4% respectively, revealing its excellent monitoring effect. To this end, the as-prepared e-skin presented multiple stimuli-perception behaviors and showed promising applications in human−machine interaction, robots, and smart diagnosis.

3.6. Application of the e-Skin-Based Intelligent Gripper. Owing to the excellent sensing and magneto-actuated features, an intelligent gripper was further designed to study its multi-field coupling sensing characteristics under complicated conditions. As shown in Figure 7a, the gripper was fabricated by assembling U-shaped conductive Ecoflex onto cross-shaped magnetic Ecoflex and then covering thermosensitive Ecoflex to form a triple-layer structure with a thickness of 1 mm. Because of the symmetry, one of the arms was selected to connect with modulus MTS to study its sensing property. In consideration of the complexity of the working environment, it was necessary to systematically study the performance under different working temperatures.

To study the thermo-resistive characteristic, the sensing performance of the gripper at different temperatures was investigated (Figure 7b,c). The human hand, attached with the gripper, bent to different degrees to grasp the cup with water temperatures of 5 and 55 °C. During the process, the color of the thermo-sensitive layer changed from indigo (room temperature) to violet (5 °C) and light grey (55 °C). At 5 °C, the resistance increased steadily (from 77.0 to 185.9 kΩ) once fingers bent to grasp the cup (Figure 7b-I), and it showed a notable growth (up to 636.7 kΩ) as the bending angle

https://dx.doi.org/10.1021/acsami.9b23547
ACS Appl. Mater. Interfaces 2020, 12, 15675−15685

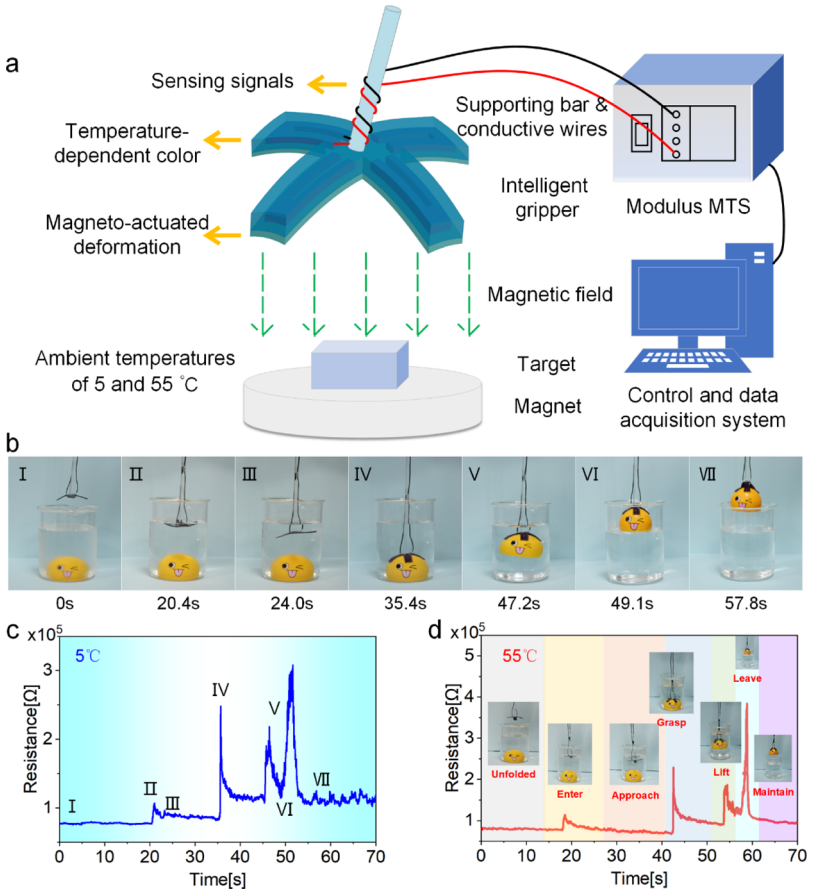

Figure 8. Multifield coupling sensing behaviors of the intelligent gripper in the process of grabbing toys actuated by magnetic field. (a) Working schematic diagram of the intelligent gripper. Photographs and resistance response at (b,c) 5 and (d) 55 °C.

increased (Figure 7b-II). However, the initial resistance changed to 65.0 kΩ when external temperature rose to 55 °C, and the corresponding resistances were 157.1 kΩ (Figure 7c-I) and 589.9 kΩ (Figure 7c-II) if grasping cups with different bending degrees. It was evident that the temperature showed a positive effect on electrical conductivity (Figure 7d). Thus, the gripper-based sensor could successfully monitor pressures and bending stimuli under various temperatures, and the resistance variations as well as the visible varying colors also could be used to quantitatively assess environmental temperatures. The thermo-resistive effect could be quantitatively analyzed by the temperature coefficient of resistance (TCR, resistance increment caused by unit temperature change).[43] The conductivity of CNT-based polymer composites was dependent on the electrically percolated network, including interconnected conductive pathways formed by nanotubes in direct contact and tunneling effect between nanotubes.[41,42] Thus, the mechanism of temperature-dependent sensing performance is proposed in Figure 7e. At high temperatures, thermal expansion of the polymer matrix reduced the effective volume fraction of CNTs, which increased the intertube distance and reduced the interconnected ECPs, thus resulting in positive TCR. On the other hand, an elevated temperature promoted the thermal vibration of electrons, which contributed to a higher transition probability for electrons with increased energy; so a negative TCR was induced.[44] Figure 7d shows a negative TCR characteristic, which demonstrated that the effect of thermal activation-enhanced tunneling effect was dominant within the range of 5−55 °C.

3.7. Multi-Field Coupling Sensing Properties of the Intelligent Gripper. Thus, because of the thermal−magnetic−mechanical responsive properties, the performance of the e-skin-based intelligent gripper was further systematically studied to explore its reliability in practical multi-field conditions. The working schematic diagram is shown in Figure 8a, in which one arm of the gripper was connected to the computer, and the arms could be actuated by an external magnetic field. As shown in Figure 8b,c, the gripper was first kept unfolded with an initial resistance of 76.4 kΩ at room temperature. Once entering water, the surface color changed from indigo to violet (Figure S7a,b), and resistance increased to 106.9 kΩ due to the disturbance of water. Then, the gripper descended to approach the target, and a higher resistance of 87.5 kΩ was observed due to the negative TCR effect. When approached, the gripper was actuated by the magnetic field to quickly fold and grasp the target within 0.34 s. Consequently, the resistance showed a significant increment (248.2 kΩ), indicating its effective deformation sensing property. Subsequently, the resistance changed to 218.4 kΩ at the moment of lifting the target. Once leaving the water, it dramatically increased to 307.6 kΩ on account of water surface tension. Finally, when it was transported out of the water, the surface color turned to indigo in seconds, and the resistance remained at 109.5 kΩ. Thus, the resistance variations could be used to assess all the deformation in the grasping process. The thermal−magnetic−mechanical coupling performance at 55 °C

https://dx.doi.org/10.1021/acsami.9b23547
ACS Appl. Mater. Interfaces 2020, 12, 15675−15685

was also investigated (Figure 8d). Similarly, the initial resistance was 77.9 kΩ, and it was reduced to 70.5 kΩ when entering hot water, revealing the negative TCR property. During the grasping process, the resistance varied to 228.9 kΩ. Finally, the surface color changed from light grey to indigo (Figure S7c), with the corresponding resistance of 97.0 kΩ. In conclusion, the intelligent gripper could effectively work in sophisticated environments with magnetic field and different temperatures. It also showed high reliable sensing properties to external working temperatures and deformations which showed promising applications in smart robots and submarine transports.

4. CONCLUSIONS

In this work, a flexible multifunctional e-skin with thermal−magnetic−mechanic tripling sensing performance was developed by assembling thermosensitive Ecoflex, magnetic Ecoflex, and conductive Ecoflex. Thermosensitive Ecoflex possessed a visual response to external temperature in a wide range (5−70 °C), and magnetic Ecoflex exhibited a high MR effect of 893.8%. Conductive Ecoflex showed excellent force-sensing capability to stretching, compressing, and bending deformations. This e-skin presented multiple force sensing performance, which could monitor tactile stimuli, weight compression, and human motions. It also exhibited magneto-actuated characteristic. Moreover, the thermo-sensitive feature also endowed it with the ability to assess the ambient temperature, and the sensing mechanism was explored. The e-skin-based intelligent gripper was proven to accomplish capturing and transporting target actuated by the magnetic field under different temperature conditions. All the external stimulations could also be assessed by the resistance variations. Therefore, this novel gripper device showed wide application prospects in wearable electronics, man−machine interaction, and intelligent driving and transport systems.

■ ASSOCIATED CONTENT

Supporting Information

The Supporting Information is available free of charge at https://pubs.acs.org/doi/10.1021/acsami.9b23547.

SEM images of thermochromic red, blue, and black fillers, CI particles, MWCNTs, Ecoflex, thermosensitive Ecoflex, magnetic Ecoflex and conductive Ecoflex; temperature-dependent colors of thermochromic red, blue, and black fillers; color reversibility of thermosensitive Ecoflex at dropping temperatures from 70 to 10 °C; curing effect of conductive Ecoflex composites with CNT mass fraction of 4.2, 4.6, and 5% after being cured at 60 °C for 4 h; the $\Delta R/R_0$ values and compression forces of 10, 30, and 100 N or tensile strains of 10, 40 and 100% as a function of time; typical sensing properties under the tensile strain of 20 and 60%; and temperature perception characteristics of the intelligent gripper when grabbing toys at 5, 25, and 55 °C (PDF)

■ AUTHOR INFORMATION

Corresponding Authors

Sheng Wang − *CAS Key Laboratory of Mechanical Behavior and Design of Materials, Department of Modern Mechanics, CAS Center for Excellence in Complex System Mechanics, University of Science and Technology of China, Hefei, Anhui 230027, PR China*; Phone: 86-551-63606382; Email: wsh160@ustc.edu.cn; Fax: 86-551-63600419

Pingan Song − *Centre for Future Materials, University of Southern Queensland, Toowoomba 4350, Australia*; orcid.org/0000-0003-1082-652X; Email: pingansong@gmail.com

Xinglong Gong − *CAS Key Laboratory of Mechanical Behavior and Design of Materials, Department of Modern Mechanics, CAS Center for Excellence in Complex System Mechanics, University of Science and Technology of China, Hefei, Anhui 230027, PR China*; orcid.org/0000-0001-6997-9526; Email: gongxl@ustc.edu.cn

Authors

Shuai Liu − *CAS Key Laboratory of Mechanical Behavior and Design of Materials, Department of Modern Mechanics, CAS Center for Excellence in Complex System Mechanics, University of Science and Technology of China, Hefei, Anhui 230027, PR China*

Shouhu Xuan − *CAS Key Laboratory of Mechanical Behavior and Design of Materials, Department of Modern Mechanics, CAS Center for Excellence in Complex System Mechanics and National Synchrotron Radiation Laboratory, University of Science and Technology of China, Hefei, Anhui 230027, PR China*; orcid.org/0000-0002-8232-9736

Shuaishuai Zhang − *CAS Key Laboratory of Mechanical Behavior and Design of Materials, Department of Modern Mechanics, CAS Center for Excellence in Complex System Mechanics, University of Science and Technology of China, Hefei, Anhui 230027, PR China*

Xiwen Fan − *CAS Key Laboratory of Mechanical Behavior and Design of Materials, Department of Modern Mechanics, CAS Center for Excellence in Complex System Mechanics, University of Science and Technology of China, Hefei, Anhui 230027, PR China*

Han Jiang − *Applied Mechanics and Structure Safety Key Laboratory of Sichuan Province, School of Mechanics and Engineering, Southwest Jiaotong University, Chengdu, Sichuan 611756, PR China*; orcid.org/0000-0003-2582-3014

Complete contact information is available at: https://pubs.acs.org/10.1021/acsami.9b23547

Notes

The authors declare no competing financial interest.

■ ACKNOWLEDGMENTS

Financial supports from the National Natural Science Foundation of China (grant nos. 11802303, 11772320, 11822209, 11972032), the Strategic Priority Research Program of the Chinese Academy of Sciences (grant no. XDB22040502), the Fundamental Research Funds for the Central Universities (grant no. WK2090050045), the China Postdoctoral Science Foundation (grant no. 2018M632543, 2019T120544), Joint Fund of USTC-National Synchrotron Radiation Laboratory (KY2090000055), and the Opening Project of Applied Mechanics and Structure Safety Key Laboratory of Sichuan Province (SZDKF-1701) are gratefully acknowledged. This study was also supported by the Collaborative Innovation Center of Suzhou Nano Science and Technology and partially carried out at the USTC Center for Micro and Nanoscale Research and Fabrication.

https://dx.doi.org/10.1021/acsami.9b23547
ACS Appl. Mater. Interfaces 2020, 12, 15675−15685

ABBREVIATIONS

e-skin, electronic skin
MREs, magnetorheological elastomers
CI, carbonyl iron
MWCNTs, multi-walled carbon nanotubes
MTS, material test system
SEM, scanning electron microscopy
ECPs, effective conductive paths
G_o, the initial storage modulus
G_s, the largest storage modulus
G_m, the magnetic-induced modulus
GF, gauge factor
TCR, temperature coefficient of resistance

REFERENCES

(1) Bae, G. Y.; Han, J. T.; Lee, G.; Lee, S.; Kim, S. W.; Park, S.; Kwon, J.; Jung, S.; Cho, K. Pressure/Temperature Sensing Bimodal Electronic Skin with Stimulus Discriminability and Linear Sensitivity. *Adv. Mater.* **2018**, *30*, 1803388−1803396.

(2) Dai, J.; Zhao, H.; Lin, X.; Liu, S.; Liu, Y.; Liu, X.; Fei, T.; Zhang, T. Ultrafast Response Polyelectrolyte Humidity Sensor for Respiration Monitoring. *ACS Appl. Mater. Interfaces* **2019**, *11*, 6483−6490.

(3) Chou, H.-H.; Nguyen, A.; Chortos, A.; To, J. W. F.; Lu, C.; Mei, J.; Kurosawa, T.; Bae, W. G.; Tok, J. B. H.; Bao, Z. A Chameleon-Inspired Stretchable Electronic Skin with Interactive Colour Changing Controlled by Tactile Sensing. *Nat. Commun.* **2015**, *6*, 8011−8021.

(4) Li, Y.; Samad, Y. A.; Liao, K. From Cotton to Wearable Pressure Sensor. *J. Mater. Chem. A* **2015**, *3*, 2181−2187.

(5) Xu, Z.; Wu, C.; Li, F.; Chen, W.; Guo, T.; Kim, T. W. Triboelectric Electronic-Skin Based on Graphene Quantum Dots for Application in Self-Powered, Smart, Artificial Fingers. *Nano Energy* **2018**, *49*, 274−282.

(6) Chortos, A.; Liu, J.; Bao, Z. Pursuing Prosthetic Electronic Skin. *Nat. Mater.* **2016**, *15*, 937−950.

(7) Qi, K.; He, J.; Wang, H.; Zhou, Y.; You, X.; Nan, N.; Shao, W.; Wang, L.; Ding, B.; Cui, S. A Highly Stretchable Nanofiber-Based Electronic Skin with Pressure-, Strain-, and Flexion-Sensitive Properties for Health and Motion Monitoring. *ACS Appl. Mater. Interfaces* **2017**, *9*, 42951−42960.

(8) Zou, B.; Chen, Y.; Liu, Y.; Xie, R.; Du, Q.; Zhang, T.; Shen, Y.; Zheng, B.; Li, S.; Wu, J.; Zhang, W.; Huang, W.; Huang, X.; Huo, F. Repurposed Leather with Sensing Capabilities for Multifunctional Electronic Skin. *Adv. Sci.* **2019**, *6*, 1801283−1801290.

(9) Wang, S.; Gong, L.; Shang, Z.; Ding, L.; Yin, G.; Jiang, W.; Gong, X.; Xuan, S. Novel Safeguarding Tactile e-Skins for Monitoring Human Motion Based on SST/PDMS−Agnw−PET Hybrid Structures. *Adv. Funct. Mater.* **2018**, *28*, 1707538−1707547.

(10) Chen, Z.; Wang, Z.; Li, X.; Lin, Y.; Luo, N.; Long, M.; Zhao, N.; Xu, J.-B. Flexible Piezoelectric-Induced Pressure Sensors for Static Measurements Based on Nanowires/Graphene Heterostructures. *ACS Nano* **2017**, *11*, 4507−4513.

(11) Zhu, G.; Yang, W. Q.; Zhang, T.; Jing, Q.; Chen, J.; Zhou, Y. S.; Bai, P.; Wang, Z. L. Self-Powered, Ultrasensitive, Flexible Tactile Sensors Based on Contact Electrification. *Nano Lett.* **2014**, *14*, 3208−3213.

(12) Yoon, S. G.; Park, B. J.; Chang, S. T. Highly Sensitive Piezocapacitive Sensor for Detecting Static and Dynamic Pressure Using Ion-Gel Thin Films and Conductive Elastomeric Composites. *ACS Appl. Mater. Interfaces* **2017**, *9*, 36206−36219.

(13) Gerratt, A. P.; Michaud, H. O.; Lacour, S. P. Elastomeric Electronic Skin for Prosthetic Tactile Sensation. *Adv. Funct. Mater.* **2015**, *25*, 2287−2295.

(14) Li, H.; Sinha, T. K.; Oh, J. S.; Kim, J. K. Soft and Flexible Bilayer Thermoplastic Polyurethane Foam for Development of Bioinspired Artificial Skin. *ACS Appl. Mater. Interfaces* **2018**, *10*, 14008−14016.

(15) Wu, H.; Su, Z.; Shi, M.; Miao, L.; Song, Y.; Chen, H.; Han, M.; Zhang, H. Self-Powered Noncontact Electronic Skin for Motion Sensing. *Adv. Funct. Mater.* **2018**, *28*, 1704641−1704651.

(16) Wang, S.; Xuan, S.; Liu, M.; Bai, L.; Zhang, S.; Sang, M.; Jiang, W.; Gong, X. Smart Wearable Kevlar-Based Safeguarding Electronic Textile with Excellent Sensing Performance. *Soft Matter* **2017**, *13*, 2483−2491.

(17) Lipomi, D. J.; Vosgueritchian, M.; Tee, B. C.-K.; Hellstrom, S. L.; Lee, J. A.; Fox, C. H.; Bao, Z. Skin-Like Pressure and Strain Sensors Based on Transparent Elastic Films of Carbon Nanotubes. *Nat. Nanotechnol.* **2011**, *6*, 788−792.

(18) Gong, S.; Schwalb, W.; Wang, Y.; Chen, Y.; Tang, Y.; Si, J.; Shirinzadeh, B.; Cheng, W. A Wearable and Highly Sensitive Pressure Sensor with Ultrathin Gold Nanowires. *Nat. Commun.* **2014**, *5*, 3132−3140.

(19) Liang, J.; Li, L.; Tong, K.; Ren, Z.; Hu, W.; Niu, X.; Chen, Y.; Pei, Q. Silver Nanowire Percolation Network Soldered with Graphene Oxide at Room Temperature and Its Application for Fully Stretchable Polymer Light-Emitting Diodes. *ACS Nano* **2014**, *8*, 1590−1600.

(20) Qiao, Y.; Wang, Y.; Tian, H.; Li, M.; Jian, J.; Wei, Y.; Tian, Y.; Wang, D.-Y.; Pang, Y.; Geng, X.; Wang, X.; Zhao, Y.; Wang, H.; Deng, N.; Jian, M.; Zhang, Y.; Liang, R.; Yang, Y.; Ren, T.-L. Multilayer Graphene Epidermal Electronic Skin. *ACS Nano* **2018**, *12*, 8839−8846.

(21) Kim, S. H.; Jung, S.; Yoon, I. S.; Lee, C.; Oh, Y.; Hong, J. M. Ultrastretchable Conductor Fabricated on Skin-Like Hydrogel−Elastomer Hybrid Substrates for Skin Electronics. *Adv. Mater.* **2018**, *30*, 1800109−1800117.

(22) Wei, P.; Yang, X.; Cao, Z.; Guo, X. L.; Jiang, H.; Chen, Y.; Morikado, M.; Qiu, X.; Yu, D. Flexible and Stretchable Electronic Skin with High Durability and Shock Resistance via Embedded 3D Printing Technology for Human Activity Monitoring and Personal Healthcare. *Adv. Mater. Technol.* **2019**, *4*, 1900315−1900324.

(23) Xu, S.; Vogt, D. M.; Hsu, W.-H.; Osborne, J.; Walsh, T.; Foster, J. R.; Sullivan, S. K.; Smith, V. C.; Rousing, A. W.; Goldfield, E. C.; Wood, R. J. Biocompatible Soft Fluidic Strain and Force Sensors for Wearable Devices. *Adv. Funct. Mater.* **2019**, *29*, 1807058−1807072.

(24) Macharia, D. K.; Ahmed, S.; Zhu, B.; Liu, Z.; Wang, Z.; Mwasiagi, J. I.; Chen, Z.; Zhu, M. UV/NIR-Light-Triggered Rapid and Reversible Color Switching for Rewritable Smart Fabrics. *ACS Appl. Mater. Interfaces* **2019**, *11*, 13370−13379.

(25) Zhao, W.; Pang, H.; Gong, X. Novel Magnetorheological Plastomer Filled with NdFeB Particles: Preparation, Characterization, and Magnetic−Mechanic Coupling Properties. *Ind. Eng. Chem. Res.* **2017**, *56*, 8857−8863.

(26) Ren, X.; Pei, K.; Peng, B.; Zhang, Z.; Wang, Z.; Wang, X.; Chan, P. K. L. A Low- Operating-Power and Flexible Active-Matrix Organic-Transistor Temperature-Sensor Array. *Adv. Mater.* **2016**, *28*, 4832−4838.

(27) Bolson, N.; Singh, D.; Lube, V.; Lubineau, G. All-Polymer Based Polymorph Skin with Controllable Surface Texture. *Smart Mater. Struct.* **2019**, *28*, 075011−075019.

(28) Jiang, Y.; Wang, Y.; Mishra, Y. K.; Adelung, R.; Yang, Y. Stretchable CNTs-Ecoflex Composite as Variable-Transmittance Skin for Ultrasensitive Srain Sensing. *Adv. Mater. Technol.* **2018**, *3*, 1800248−1800255.

(29) Gao, W.; Wang, X. Steady Shear Characteristic and Behavior of Magneto-Thermo-Elasticity of Isotropic MR Elastomers. *Smart Mater. Struct.* **2016**, *25*, 025026−025035.

(30) Gao, W.; Wang, X. Experimental and Theoretical Investigations on Magnetoelastic Shear Behavior of Isotropic MR Elastomers under Gradient Magnetic Fields. *J. Magn. Magn. Mater.* **2019**, *483*, 196−204.

(31) Feng, J.; Xuan, S.; Ding, L.; Gong, X. Magnetoactive Elastomer/PVDF Composite Film Based Magnetically Controllable Actuator with Real-Time Deformation Feedback Property. *Composites, Part A* **2017**, *103*, 25−34.

(32) Böse, H.; Rabindranath, R.; Ehrlich, J. Soft Magnetorheological Elastomers as New Actuators for Valves. *J. Intell. Mater. Syst. Struct.* **2012**, *23*, 989−994.

https://dx.doi.org/10.1021/acsami.9b23547
ACS Appl. Mater. Interfaces 2020, 12, 15675−15685

(33) Hu, T.; Xuan, S.; Ding, L.; Gong, X. Stretchable and Magneto-Sensitive Strain Sensor Based on Silver Nanowire-Polyurethane Sponge Enhanced Magnetorheological Elastomer. *Mater. Des.* **2018**, *156*, 528−537.
(34) Akhavan, H.; Ghadiri, M.; Zajkani, A. A New Model for the Cantilever MEMS Actuator in Magnetorheological Elastomer Cored Sandwich Form Considering the Fringing Field and Casimir Effects. *Mech. Syst. Signal Process.* **2019**, *121*, 551−561.
(35) Li, M.; Wang, Y.; Zhang, Y.; Zhou, H.; Huang, Z.; Li, D. Highly Flexible and Stretchable MWCNT/HEPCP Nanocomposites with Integrated Near-IR, Temperature and Stress Sensitivity for Electronic Skin. *J. Mater. Chem. C* **2018**, *6*, 5877−5887.
(36) Charaya, H.; La, T. G.; Rieger, J.; Chung, H. J. Thermochromic and Piezocapacitive Flexible Sensor Array by Combining Composite Elastomer Dielectrics and Transparent Ionic Hydrogel Electrodes. *Adv. Mater. Technol.* **2019**, *4*, 1900327−1900336.
(37) Huang, P.; Li, Y.-Q.; Yu, X.-G.; Zhu, W.-B.; Nie, S.-Y.; Zhang, H.; Liu, J.-R.; Hu, N.; Fu, S.-Y. Bioinspired Flexible and Highly Responsive Dual-Mode Strain/Magnetism Composite Sensor. *ACS Appl. Mater. Interfaces* **2018**, *10*, 11197−11203.
(38) Wang, S.; Xuan, S.; Jiang, W.; Wei, F. J.; Yan, L.; Mao, Y.; Mei, L.; Gong, X. Rate-dependent and Self-healing Conductive Shear Stiffening Nanocomposite: A Novel Safe-guarding Material with Force Sensitivity. *J. Mater. Chem. A* **2015**, *3*, 19790−19799.
(39) Lokander, M.; Stenberg, B. Performance of Isotropic Magneto-rheological Rubber Materials. *Polym. Test.* **2003**, *22*, 245−251.
(40) Lokander, M.; Stenberg, B. Improving the Magnetorheological Effect in Isotropic Magnetorheological Rubber Materials. *Polym. Test.* **2003**, *22*, 677−680.
(41) Yuan, F.; Wang, S.; Zhang, S.; Wang, Y.; Xuan, S.; Gong, X. A Flexible Viscoelastic Coupling Cable with Self-adapted Electrical Properties and Anti-impact Performance toward Shapeable Electronic Devices. *J. Mater. Chem. C* **2019**, *7*, 8412−8422.
(42) Jiang, M.-J.; Dang, Z.-M.; Xu, H.-P. Significant Temperature and Pressure Sensitivities of Electrical Properties in Chemically Modified Multiwall Carbon Nanotube/Methylvinyl Silicone Rubber Nanocomposites. *Appl. Phys. Lett.* **2006**, *89*, 182902−182905.
(43) Cen-Puc, M.; Oliva-Avilés, A. I.; Avilés, F. Thermoresistive Mechanisms of Carbon Nanotube/Polymer Composites. *Phys. E* **2018**, *95*, 41−50.
(44) Shen, J. T.; Buschhorn, S. T.; De Hosson, J. T. M.; Schulte, K.; Fiedler, B. Pressure and Temperature Induced Electrical Resistance Change in Nano-Carbon/Epoxy Composites. *Compos. Sci. Technol.* **2015**, *115*, 1−8.

https://dx.doi.org/10.1021/acsami.9b23547
ACS Appl. Mater. Interfaces 2020, 12, 15675−15685